Design for a cruciform coupon used for tensile biaxial transverse tests on composite materials

E. Correa*, A. Barroso, M.D. Pérez, F. París

Elasticity and Strength of Materials Group, Continuum Mechanics Department, School of Engineering, University of Seville, Spain.

*Corresponding author ecorrea@us.es

ABSTRACT

This paper focuses on the design of the appropriate geometry for cruciform coupons conceived to be tested under tensile biaxial transverse loads. To this end, Finite Element models were developed and their results were used to propose a geometry which minimizes undesirable effects such as stress concentrations, develops a uniform state of biaxial stresses in the central zone of the coupon and assures that the failure takes place at this zone. The experimental results confirm the validity of the numerical models.

KEYWORDS: C. Finite element analysis. C. Transverse cracking. Cruciform coupon.

1. INTRODUCTION

The significant use of composite materials in the industry has been accompanied over the last few years by an increase in terms of responsibility that these materials hold in the components they are part of. As a consequence, it is essential that advances are made in our understanding of the mechanisms of damage affecting these materials as well as in the prediction of their possible appearance.

This study focuses on transverse failure, known as matrix/inter-fibre failure at lamina level. Such failure may appear in unidirectional laminates under transverse loads or in

multidirectional laminates subjected, for example, to impact loads. Illustrative is the unfolding failure that laminates of composite may suffer, combined with internal delamination, with the presence of intralaminar cracks that appear under biaxial stress states. This failure, captured by ILTS (Inter Laminar Tensile Strength) test, appears for instance in joining parts of an aircraft fuselage. The prompt appearing of this failure, as the fibre is not involved in it, makes both the determination of the stresses as the corresponding allowables involved in the failure, a critical point to improve the performance of composites under failure of this type.

Matrix failure under tension has already been studied at micromechanical level by París et al [1] and Correa et al [2-3] using BEM models. These numerical studies made it possible to identify the initial phases of damage growth at micromechanical level as well as subsequent phases of growth leading to macromechanical failure. Many of the existing proposals for the prediction of matrix failure at lamina level are based on the hypothesis that the failure occurring at a plane is governed by the components of the stress vector associated with that plane (see for instance Hashin and Rotem [4]). This assumption was revised by París et al [5] and Correa et al [6] for the case under tension. The results obtained showed that the presence of a secondary tension, perpendicular to the tension nominally responsible for the failure, could alter some aspects of the failure phases previously detected for the uniaxial case; particularly, it was concluded that this secondary tension (which is normal to the originally assumed plane of failure) could slightly delay the appearance of failure.

It seems necessary, therefore, to check the validity of the conclusions derived from the aforementioned micromechanical numerical studies by means of macromechanical experimental tests. Specifically, experimental studies should be carried out on coupons extracted from unidirectional laminates and subjected to transverse biaxial loads. This

task was initiated by the authors in [5] through the development of tension-compression transverse tests, and subsequently continued in Barroso et al [7,8], where the design and development of a reliable low-cost biaxial device to be used in any standard uniaxial testing machine was presented.

Tension-compression transverse tests do not require special coupons since tension is applied in a regular way and compression is applied laterally to the coupon. However, in loading situations in which both transverse loads are tensile-type, the geometry of the coupon required for the development of the experimental tests needs to be cruciform in order to be able to introduce the load along two perpendicular axes. The design of this coupon can be performed using FEM models, intending to reproduce the behaviour of the coupon under biaxial loading cases. Notice that the particular orientation of the fibre in this case (which is normal to the testing plane) hardly complicates the coupons manufacturing process from both a technical and economical point of view; therefore, this feature needs to be taken into consideration in the previous design process.

The objective of this paper is the development of FEM models, Section 2, used to design the appropriate geometry of a cruciform coupon to be subjected to tensile-tensile transverse tests. Preliminary studies are developed in Section 3.1, their results being supported by experimental tests described in Section 3.2 to check the representativity of FEM models. Once the models are validated, the final numerical studies carried out to optimize the coupon morphology are presented in Section 4.

2. MODELS

The following requirements must be taken into account for the design of a coupon which will be subjected to tension-tension transverse biaxial loads:

- The development of a uniform state of biaxial stresses on the coupon under testing, in the area susceptible of failure.

- The maximization of the area nominally subjected to biaxial stresses.

- The minimization of the possible stress concentrations derived from the geometry.

- The failure occurrence in the zone subjected to a uniform state of biaxial stresses.

Finding a geometry that simultaneously fulfils these aspects is not a simple task. A great number of interesting studies concerning cruciform coupons already exists in the literature (see for example Welsh and Adams [9], Bhatnagar et al [10], Smits et al [11], Lamkanfi et al [12-13], Makris et al [14], Escárpita et al [15] and Huang et al [16]). However, the authors of the present paper have not found a specific design for unidirectional laminates subjected to loads transverse to the direction of the fibres (i.e. 90º coupons). Discovering the appropriate geometry for transverse tests in composites involves a real challenge from both the design and manufacturing point of view.

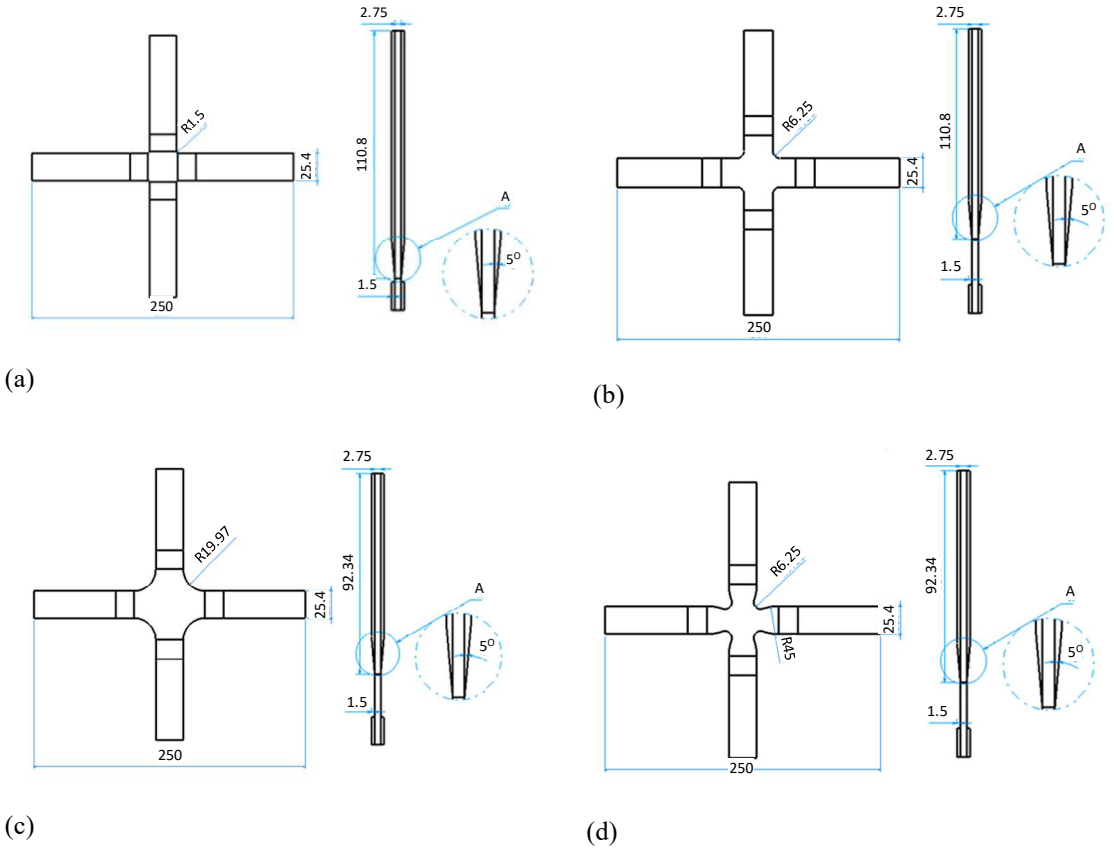

Figure 1. Geometric proposals: Type (a) A, (b) B, (c) C and (d) D coupons

(dimensions in mm).

Four initial geometrical models are considered in this paper, Types A, B, C and D coupons, Fig. 1. All of them are composed of a main body of constant thickness, which represents the cruciform coupon itself manufactured from a unidirectional laminate, and 8 reinforcing tabs (one at each side of the "arms" of the coupon). The first three models (A, B and C) were thought to be the simplest cruciform proposals from the manufacturing point of view, since they shows a single fillet radius, R, in the central zone (in particular, R(A)= 1.5mm, R(B)= 6.25mm and R(C)= 19.97mm). On the other hand, Type D coupon constitutes an evolved proposal which, based on [11], presents 2 fillet radii in the central zone, see Fig. 1d. On all types the arms are reinforced with tabs whose slope allows a soft transition of the stress state to the central zone of the coupon. These tabs have a double function: firstly, they ensure that the coupon is adequately fixed to the machine grips during testing, and secondly, in order to promote failure initiation at the central zone of the coupon (i.e. the zone nominally subjected to biaxial loads), they guarantee a thickness increase of the coupon away from the zone of interest.

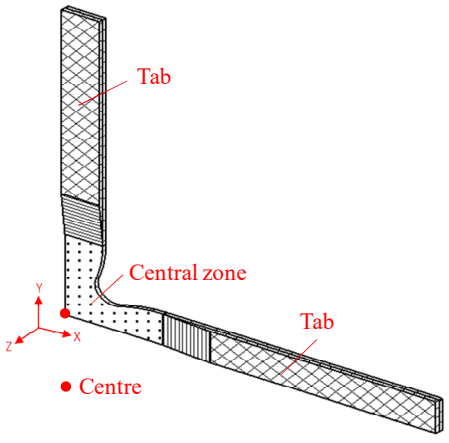

Figure 2. Type D 3D geometrical model schematically showing fibre orientation.

On all types of coupon considered the laminate chosen corresponds to a carbon-epoxy system (AS4/3501-6), which properties are specified in Soden et al [17], whereas tabs are manufactured from glass fibre +45/-45 fabric.

As can be observed in Fig. 1 the four geometrical proposals present triple symmetry; therefore only an eighth part of the entire coupon is modelled. As an example, Type D coupon is schematically depicted in Fig. 2, where the reference system, fibre orientation and nomenclature of some parts of the model are included.

A 3D FEM model, considering the orthotropic properties of the material and using commercial software Patran/Nastran, was prepared for each geometry proposed, in order to study the stress state experienced, under the combined action of two external transverse tensions, acting respectively at the ends of both the horizontal (x-axis) and vertical (y- axis) arms. Different loading cases were considered, all of them corresponding to a fixed value of the external tension σ_0 applied at the edge of the horizontal arm, and different portions of σ_0 (characterized by a coefficient $n = 0.1, 0.25, 0.5, 0.75$ and 1) at the edge of the vertical arm.

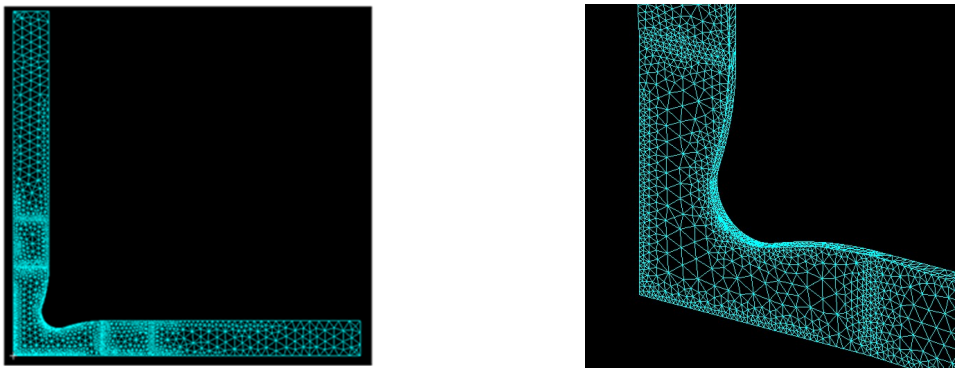

Figure 3. 3D mesh employed for Type D coupon.

Therefore, the limit case $n = 0$ would correspond to the uniaxial case (in which only an external tension of value σ_0 is applied at the edge of the horizontal arm), whereas $n = 1$ represents the symmetrical biaxial case in which σ_0 is applied at the edge of both

arms. σ_0 was taken as being equal to the transverse tensile strength (Y_T) associated with the material considered, 48 MPa in this case (Soden et al [17]).

Linear elastic behaviour is assumed. 10 nodes-tetrahedral elements of quadratic order are employed. With reference to the mesh size, a number of 21000 elements were approximately employed for each model. A view of the mesh used for Type D coupon can be observed in Fig. 3.

3. PRELIMINARY STUDIES

3.1 FEM results

The stress states associated with the different loading cases considered were analyzed for each type of coupon. Focusing our attention on the tension-tension (T-T) case ($n=1$) the results show that σ_{xx} and σ_{yy} are the dominant stresses, presenting symmetrical distributions with reference to the x-y plane bisector. Notice that these stresses correspond to σ_{22} and σ_{33} in material axes and the material is nominally isotropic in the x-y plane.

σ_{xx} distribution is shown in Fig. 4 for the different coupon types, where a zoom of the central zone is also included. The same scale of representation is used on all the cases for purposes of comparison, extending from the maximum tensile value obtained (occurring at Type A coupon) to the maximum compressive value found (occurring at Type D coupon). Stress concentrations are found at the free edge on the four coupons, the maximum value occurring for Type B (290 MPa) followed by Types D (205 MPa), A (160 MPa) and C (149 MPa). These results are summarized in Table 1 where σ_{xx}^{max} (the maximum value of σ_{xx} at the free edge), σ_{xx}^{centre} (σ_{xx} value at the centre of the

coupon, see Fig. 2), and the ratio between both values, $\sigma_{xx}^{max} / \sigma_{xx}^{centre}$ (representing the concentration factor), are compiled.

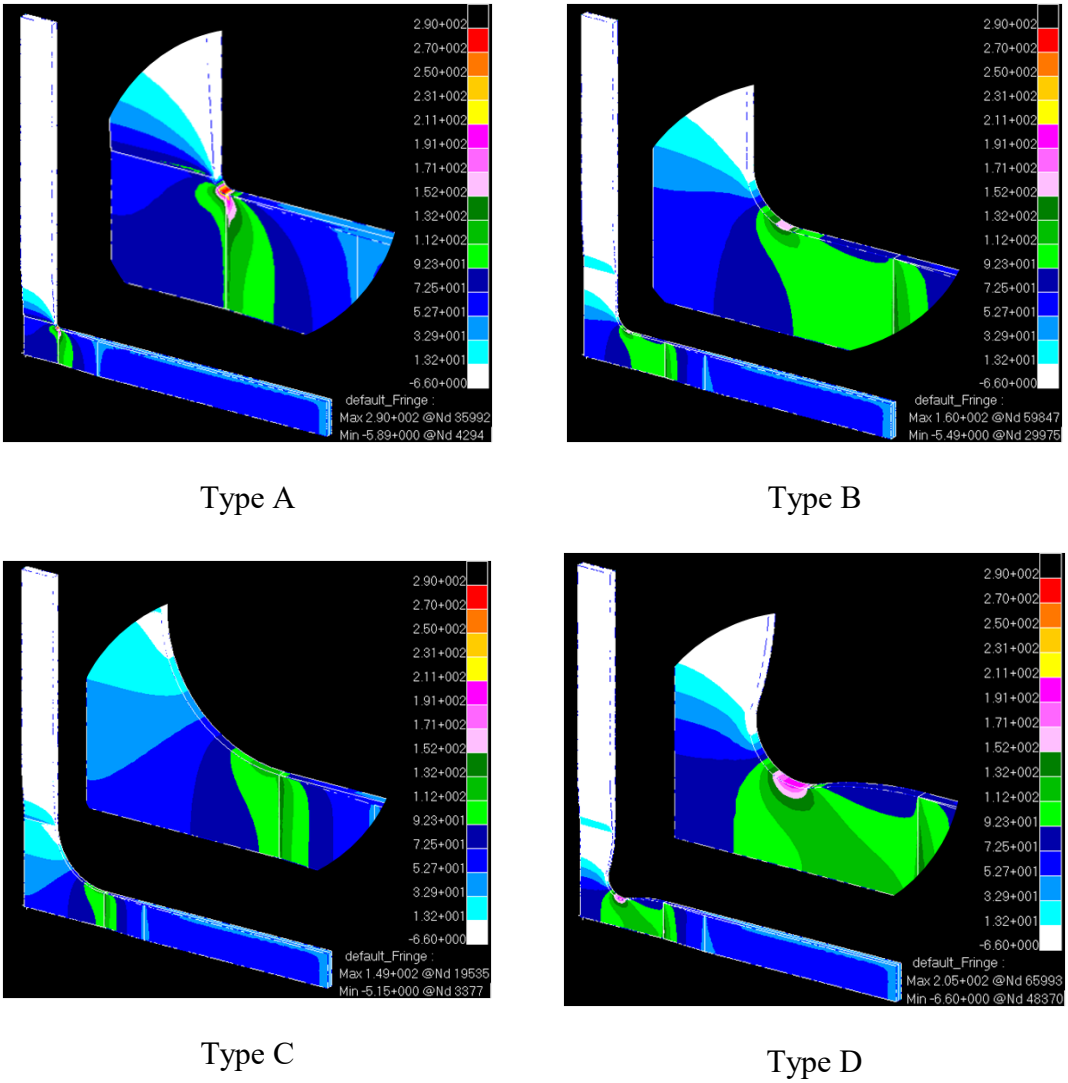

Figure. 4. σ_{xx} distribution (MPa) for Type A, B, C and D coupons ($n = 1$).

Tensile values are found for σ_{xx} at all points of the central zone of the specimen as well as along the horizontal arm of the coupons. Almost negligible compressive values appear along the vertical arm of the coupons, this zone is shown in white in the Figure.

Looking at Type A coupon, a uniform σ_{xx} distribution is detected at its central zone even though its value is only of an order of 25% of the maximum tension encountered at the free edge, i.e. $\sigma_{xx}^{\max} / \sigma_{xx}^{centre} = 3.88$. Besides, high tensions are also vertically

distributed along the horizontal tab border and this would eventually lead to failure out of the biaxial zone.

Using a higher curvature radius, Type B coupon, reduces the difference between σ_{xx} values at the central zone and the maximum σ_{xx} at the free edge, though still being quite significant ($\sigma_{xx}^{\max} / \sigma_{xx}^{centre} = 2.32$). High tensions are also distributed vertically along the horizontal tab border and extending as well to part of the central zone in this case.

With reference to the σ_{xx} distribution associated with Type C coupon, this is very similar to that shown by Type B, although the stress concentration, and therefore the maximum tensile value, moves towards the horizontal arm. Moreover, the stress value at the centre of the coupon is only 36% of such maximum ($\sigma_{xx}^{\max} / \sigma_{xx}^{centre} = 2.76$).

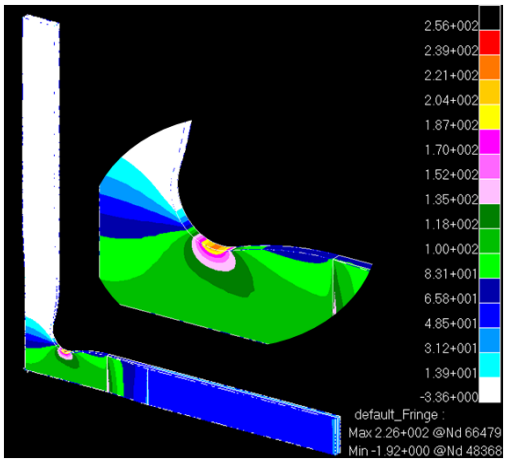

$n = 0.25$

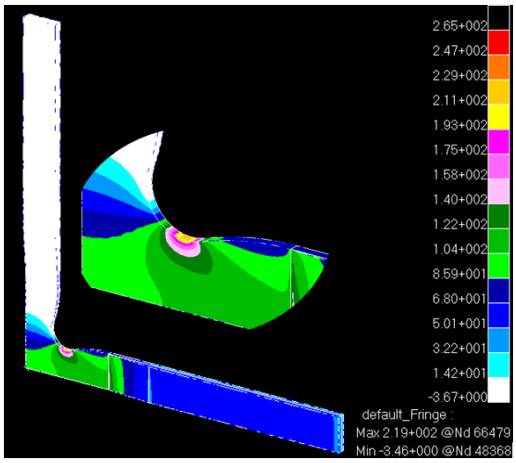

$n = 0.5$

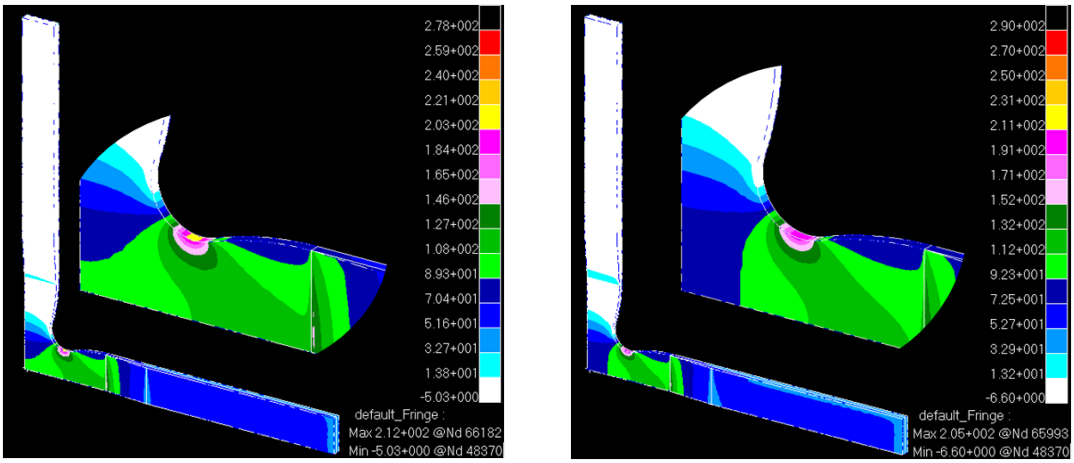

$n = 0.75$ $n = 1$

Figure 5. σ_{xx} distribution (MPa) for Type D coupon ($n = 0.25, 0.5, 0.75$ and 1).

Notice that the foreseeable decreasing tendency detected for both σ_{xx}^{max} and σ_{xx}^{centre} from Type A to Type C contrasts with the greater $\sigma_{xx}^{max} / \sigma_{xx}^{centre}$ ratio calculated for Type C (2.76) versus Type B (2.38). The increase of this ratio (with a clear mathematical explanation) may be physically related to the differences existing between both coupons in the local geometry of the free edge (in addition to the value of the fillet radius).

Finally, Type D coupon presents a relationship between $\sigma_{xx}^{\max}$ and σ_{xx}^{centre} similar to that already encountered for Type B coupon (42%, $\sigma_{xx}^{\max} / \sigma_{xx}^{centre} = 2.38$); high σ_{xx} values are also found at the biaxial zone, although they do not reach the centre of the coupon.

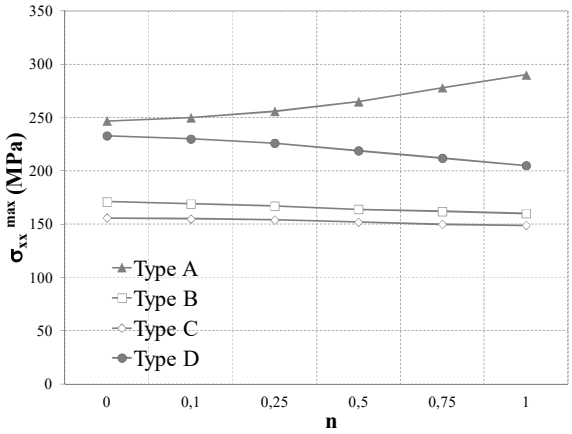

Figure 6. σ_{xx}^{max} versus the secondary external tension for Type A, B, C and D coupons.

Additional characteristics of the coupons behaviour have been studied when the value of n coefficient is varied. As an example, Fig. 5 presents σ_{xx} distribution of Type D coupon for $n = 0.25, 0.5, 0.75$ and 1 (notice the different scale). A summary of the main conclusions encountered follows:

- σ_{xx} (symmetrical to σ_{yy} for $n = 1$) is the dominant stress for all coupons and the whole range of n coefficient considered.
- Relevant stress concentrations are detected for σ_{xx} at the centre of the free edge, except for Type C, in which the concentration is located at the joint between the tab and the coupon arm. This concentration decreases as n coefficient evolves from 1 to 0.
- σ_{xx} values at the central zone decrease as the secondary external tension increases.
- In general, σ_{xx} distribution at the central zone of the coupons is quite uniform.
- As expected, σ_{yy} values increase as the secondary external tension increases.
- σ_{xy} is negligible in the central zone for all coupons.

Fig. 6 shows the maximum values detected for each type of coupon versus n. It can be confirmed from Fig. 6 that Type B and C coupons σ_{xx}^{max} seems to be independent of n.

As a summary, the results described lead to the rejection of Types A and C due to the following: first, the higher values of their concentration factor (see Table 1), and second, the expected zone of failure initiation (which seems to occur at the zone under uniaxial tension (arm) for both coupons if the maximum stress criterion is assumed, Fig. 4).

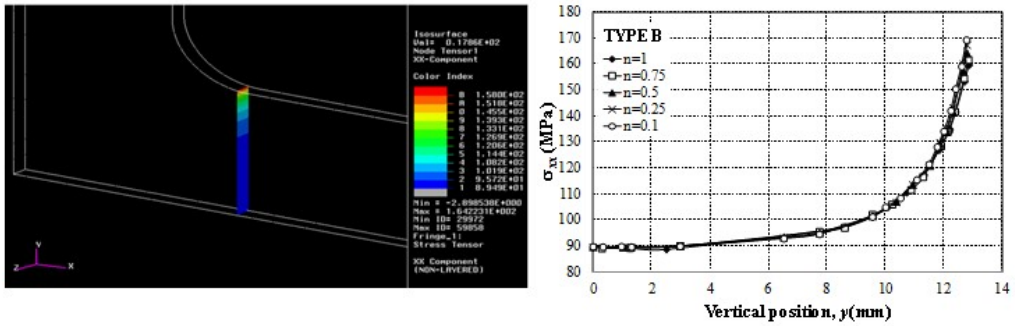

Figure 7. Type B coupon. (a) σ_{xx} distribution along the theoretical failure surface ($n = 0.5$), (b) σ_{xx} versus y ($n = 0.1, 0.25, 0.5, 0.75$ and 1).

With reference to Type B and D coupons a better behaviour is observed: lower values for the concentration factor are detected and the σ_{xx} highest values (except for the concentration at the free edge) are located partially at the central zone (Type D) or quite close to it (Type B). This behaviour, however, is not sufficient to choose any of them as a final design, since failure initiation is expected to be promoted by the free edge stress concentration. Therefore, geometrical modifications are required.

Coupon	σ_{xx}^{max}	σ_{xx}^{centre}	$\sigma_{xx}^{max} / \sigma_{xx}^{centre}$
Type A	290	74.7	3.88
Type B	160	69	2.32
Type C	149	53.9	2.76
Type D	205	86.2	2.38

Table 1. $\sigma_{xx}^{max} / \sigma_{xx}^{centre}$ for Type A, B, C and D coupons ($n = 1$).

In order to decide whether to select coupon B or D to perform the geometrical modifications, a more detailed analysis of the zone where the failure might start is undertaken. To this end, an initial assumption about a theoretical failure surface is defined, based on the maximum stress criterion. This failure surface is defined as a

plane parallel to the yz plane and starts at the node where maximum σ_{xx} is detected. It is important to remark that results obtained also show that σ_{xy}, although negligible at the central zone of the specimens, could reach significant values at the stress concentration area, in fact of an order of $0.4\sigma_{xx}$. Nevertheless, the application of the maximum stress criterion leads to the comparison between the σ_{xx}/Y_T and σ_{xy}/S_T ratios. S_T has been considered by some authors (Puck and Schürman [18]) to approximately take the value of $0.5Y_C$. For the material under study, Y_T is 48 MPa, Y_C is 200 MPa (Soden et al [17]), consequently $S_T \cong 100MPa$. Then, based on these values of the material properties, σ_{xx}/Y_T ratio would control the fracture process in all loading cases, under the assumption of the maximum stress criterion. Notice that the consideration of an alternative quadratic criterion (see for instance Puck and Schürmann [18]) could even reinforce the dominant role of σ_{xx} (and σ_{yy} in the n=1 case) in the failure.

In Figures 7a and 8a σ_{xx} evolution along the assumed theoretical failure surface is presented for Types B and D, respectively, and for the particular case $n = 0.5$. In Figures 7b and 8b σ_{xx} distribution versus the vertical position y is plotted for Types B and D, respectively, and for $n = 0.1, 0.25, 0.5, 0.75$ and 1.

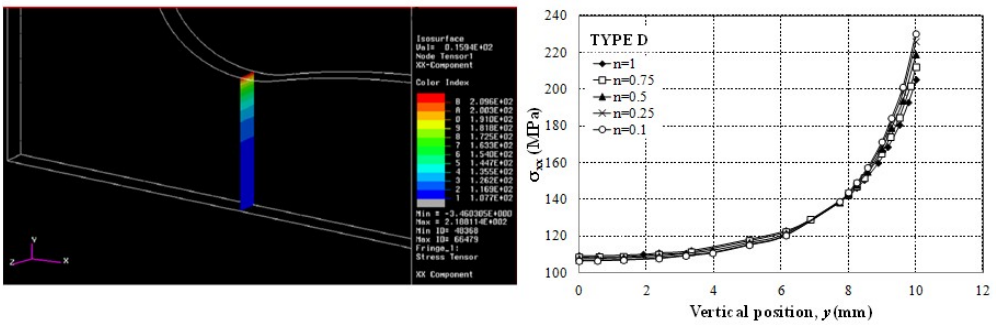

Figure 8. Type D coupon. (a) σ_{xx} distribution along the theoretical failure surface. ($n = 0.5$), (b) σ_{xx} versus y ($n = 0.1, 0.25, 0.5, 0.75$ and 1).

Looking at Figs. 7 and 8, a weak dependence on n is detected for both coupons. Moreover, higher stress values appear in Type D than in Type B. σ_{xx} distribution (Figs. 7b and 8b) versus y shows a horizontal stretch that extends until $y = 10mm$ for Type B, followed by the zone where the stress concentration starts, and thus, the σ_{xx} value quickly increases to its maximum value at the free edge. For Type D, a shorter horizontal stretch is measured ($y = 5mm$).

Finally, it is worth noting that the theoretical failure plane for Type D it is more centrally positioned than the one for Type B; this can be deduced from the results presented in Table 2, where the x coordinate, for the theoretical failure plane versus n is compiled for Type B and D coupons. It can be observed that a weak dependence on n is detected for this coordinate in both specimens.

Based on these results, the Type D coupon is chosen as the basis for a new design that, containing some geometrical modifications, will be presented in the Section 4.

	Theoretical failure surface x coordinate (mm)	
n	**Type B**	**Type D**
1	17.51	15.78
0.75	17.64	15.83
0.5	17.86	15.93
0.25	17.86	15.93
0.1	17.98	15.93

0	17.98	15.93

Table 2. Theoretical failure surface horizontal position, x coordinate (mm), for $n = 0, 0.1, 0.25, 0.5, 0.75$ and 1.

3.2 Experimental results

As mentioned above in the Introduction, the manufacturing process of cruciform specimens specifically designed for tensile-tensile transverse tests is a hard task. The particular position of the fibres (perpendicular to the plane of the coupon), the coupon dimensions and the reduced value of transverse tensile strength, strongly complicate the manufacturing process and considerably rise its costs. Consequently, as the risk of premature fracture is significantly high, a special manufacturing procedure needs to be conceived to solve these difficulties.

These reasons made it reasonable to perform experimental tests at this point (i.e. when the numerical design process has not yet been finished but several preliminary geometrical proposals have been studied) in order to check the representativity of the numerical tool. To this end, the Type D coupon was manufactured [7,8].

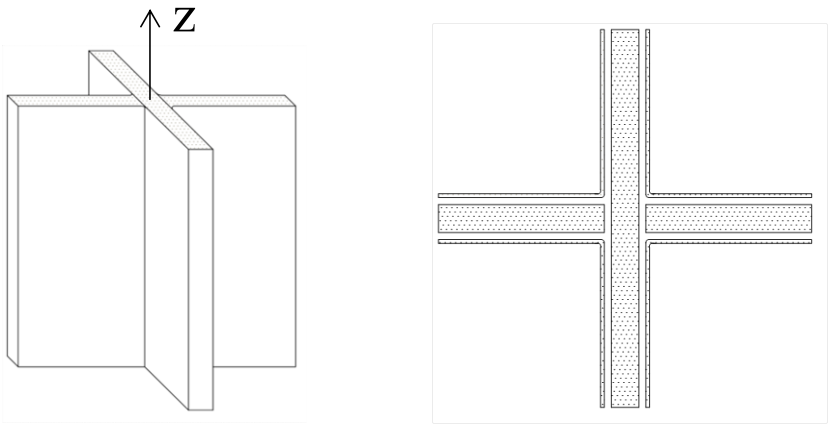

(a) (b)

Figure 9. (a) 3D view of the cruciform prism, (b) Cruciform prism with stiffener plies.

The manufacturing process starts with the building of a cruciform prism, see Fig. 9a.

The set up of the cruciform prism, where the fibres follow the z-axis direction, consist of several stages:

1) 108 carbon/epoxy pre-preg plies are laminated forming a 300x300 mm^2 unidirectional laminate.

2) The laminate is divided in two halves, and again, one of them in other two, resulting three laminates with the following dimensions: 300x150 mm^2 (vertical arm), 75x300 mm^2 (two horizontal arms), see Fig. 9b.

3) The cruciform prism is built using the three prepared arms.

4) Each side of the cruciform prism is covered with one single ply (with the same z-axis orientation of the fibres) in order to provide additional stiffness.

5) 4 aluminium blocks are employed to form a rectangular assembly that will maintain the cruciform shape during the curing stage, see Fig. 10a.

Once the rectangular assembly is prepared, it is inserted in a vacuum bag and constrained with a grip system in order to avoid misalignments during curing, Fig. 10b. Finally, the whole system is introduced in the autoclave for its curing.

Once cured, the cruciform prism is cut in slices using a water refrigerated diamond disk. The upper and lower transverse faces of these slices are polished. The curved shape of the arms junctions is obtained by the machining of the slices using a metallic sample as master copy (Fig. 11a); this master copy has been previously manufactured by numerical control tooling.

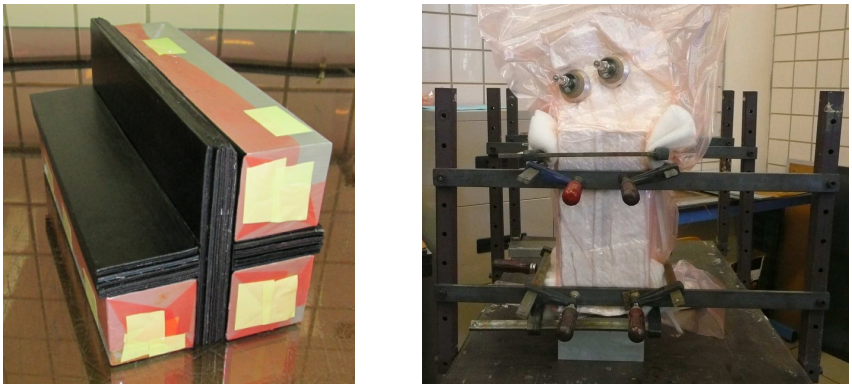

(a) (b)

Figure 10. Rectangular assembly (a) composed by the cruciform prism and the aluminum blocks (b) inserted in vacuum bag and constrained by grip system.

3.2.1 Uniaxial tests

As already explained, tensile uniaxial tests on the Type D coupon were planned in order to check the representativity of the numerical models performed, prior to the required geometrical optimization. As will be explained in the following paragraphs, the validity of the numerical tool does not compulsory require to perform biaxial tests, which carrying out entails additional difficulties.

The tests were carried out using a universal tests machine, Fig. 11b; the shape and location of the failure plane was observed and, based on the measurements provided by strain gauges, the stress state at failure in the coupon centre was calculated (mean value of 30.8MPa and standard deviation of 0.6MPa).

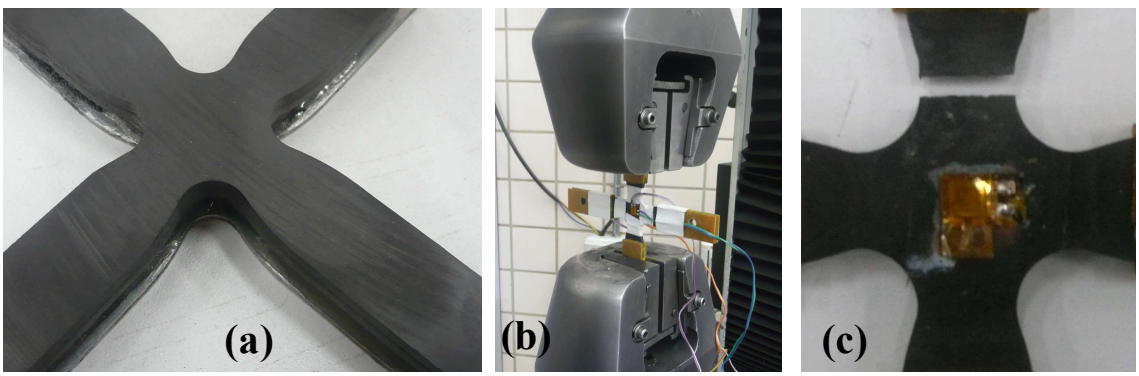

Figure 11. Type D coupon. (a) manufactured, (b) under tensile uniaxial test, (c) tested.

The results obtained were compared with the value of the transverse tensile strength of the material, Y_T (mean value of 60.4MPa and standard deviation of 4.6MPa), also experimentally measured from complementary tests performed on regular rectangular coupons.

The tests results obtained firstly help to confirm that the cruciform sample failure occurs, as expected, in the direction perpendicular to the load applied and out of the central zone of the sample (Fig. 11c), and, as already predicted by the FEM models (Fig.8), the failure follows the plane promoted by the stress concentration located at the free edge.

Secondly, the $\sigma_{xx}^{max} / \sigma_{xx}^{centre}$ ratio was calculated from the results of the experimental tests assuming that $\sigma_{xx}^{\max}$ at the free edge coincides with Y_T measured in the tensile uniaxial transverse tests on rectangular specimens; σ_{xx}^{centre} was calculated from the measurement of the strain gauges when failure occurs and making use of the constitutive equations for generalized plane stress. $\sigma_{xx}^{max} / \sigma_{xx}^{centre}$ determined in this way takes the experimental value of 2. If the results of the FEM model associated with n=0 case (partially presented in Fig. 6 and Table 2) are used to calculate this ratio, the value obtained is 2.1. Thus, an excellent agreement between both values (experimental and numerical) exists, which validates the results of the numerical models and enables the numerical models to predict the coupons behaviour prior to their manufacture and testing.

Notice that the consistency of the previous reasoning is based on the fact that in accordance with the FEM model results, the area affected by the stress concentration (where the failure appears experimentally) has a size of 3.7 mm^2, which implies an area

that approximately involves 3000 fibres, and this in addition to the almost constant value of the stress in the area of concentration, makes consistent the application of a failure criterion based on macro-stresses in the area of interest.

3.2.1 Biaxial tests

Although the Type D geometry was not optimized, tensile biaxial tests on these coupons were carried out using a mechanical device, designed and manufactured by the authors, adapted to a universal (uniaxial) testing machine, see Fig. 12 (Barroso et al [7]). The aim of this testing campaign was, first, to confirm the proper operation of the coupon on the mechanical device and, second, to check the adequacy of the biaxial numerical predictions presented in Section 3.1 for this configuration, in particular, the orientation and position of the plane of failure.

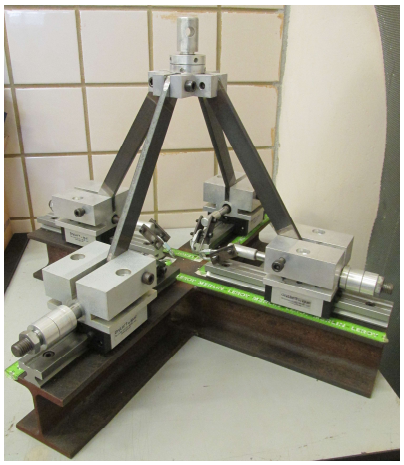

Figure 12. Device employed for biaxial tests.

A set of 19 coupons was tested. Special care was devoted to control the bending parameter in both loading axes. Monitoring of this bending parameter (measured following ASTM E1012 standard) was performed by means of strain gages at both sides of the coupon and both loading directions (x and y).

Fig. 13a shows the value of the bending parameter, for both loading axes during the test of one coupon (representative of the whole set), in particular, number 15. It is

important to guarantee a satisfactory bending parameter at the instant of failure if the influence of the biaxiality in failure wants to be studied. In this sense, as can be observed in Fig. 13a, the value of the bending parameter is below 5% for almost the entire test, and specially low (1% or 2%) at failure. A very similar evolution was found in the rest of the tests performed, then confirming the excellent behavior of the device in terms of the bending parameter.

The coupons were tested under tensile biaxial loads with different values of *n* coefficient. The results show that the failure path of all coupons seems to be associated with the stress concentration at the free edge and following the transverse direction previously predicted by the FEM model (Section 3.1). This can be observed in Fig. 13b where an image of coupon number 15 (n=0.96), once tested, is presented. This conclusion helps to confirm, once more (see Section 3.2.1), the representativity of the numerical predictions and the validity of the numerical tool employed in the design of the cruciform coupon.

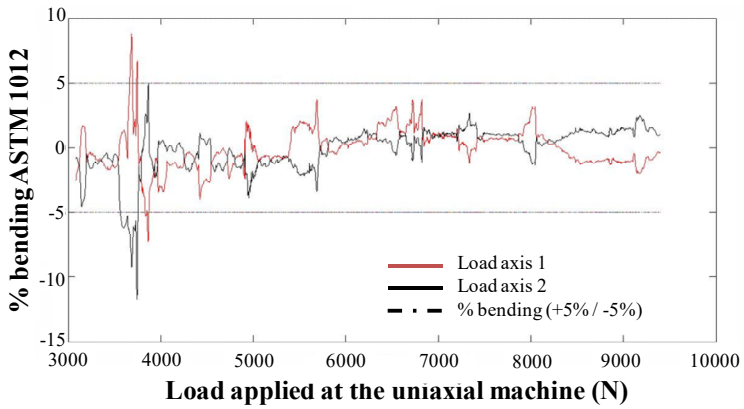

(a)

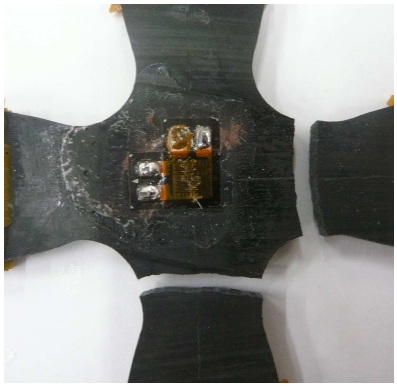

(b)

Figure 13. (a) Bending parameter during the test, (b) Broken coupon.

With reference to the stress results, Fig. 14 represents σ_{xx} at the centre of the coupon versus the stress ratio (n_σ).

n_σ is defined by $n_\sigma = \sigma_{yy}^a + \sigma_{yy}^b \big/ \sigma_{xx}^a + \sigma_{xx}^b$ where $\sigma_{xx}^a, \sigma_{xx}^b, \sigma_{yy}^a, \sigma_{yy}^b$ are the values of the normal stresses at both faces (a and b) of the coupon; these values have been calculated using the strain gages data and the 2D constitutive law in generalized plane stress. The tests performed correspond to $0.6 < n_\sigma < 1$.

As the geometry of the coupon has not yet been optimized (the failure appearing at the stress concentration areas in all cases), the value of these biaxial results is just indicative. The values of σ_{xx} are represented in Figure 14 using the information given by the strain gauges at the instant of failure. The dispersion observed is of a similar order than that in uniaxial transverse tests.

From the observation of Fig. 14, a slight decreasing tendency seems to be detected in σ_{xx} at the centre of the coupon as n increases; it is important to remark that this tendency was already predicted by the numerical model (Fig. 5).

Finally, the experimental results, in addition to confirm the validity of the FEM models, reassures the necessity of the optimization of Type D geometry, subject addressed in the next Section.

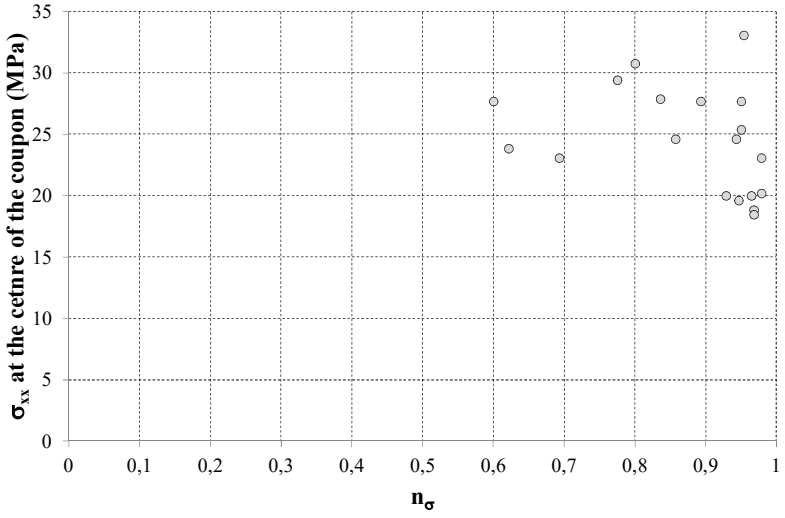

Figure 14. σ_{xx} results for the tensile biaxial tests in cruciform specimens.

4 GEOMETRICAL MODIFICATIONS

The geometrical modifications pursue the main objective of reducing the stress concentration at the free edge as well as making the stress distribution uniform at the central zone of the coupon (the area nominally subjected to biaxial loads). The final goal is, as explained in Section 2, for the failure to be originated in the central zone of the samples. This objective cannot be reached in a single step and therefore several subsequent models were explored until a final design was achieved.

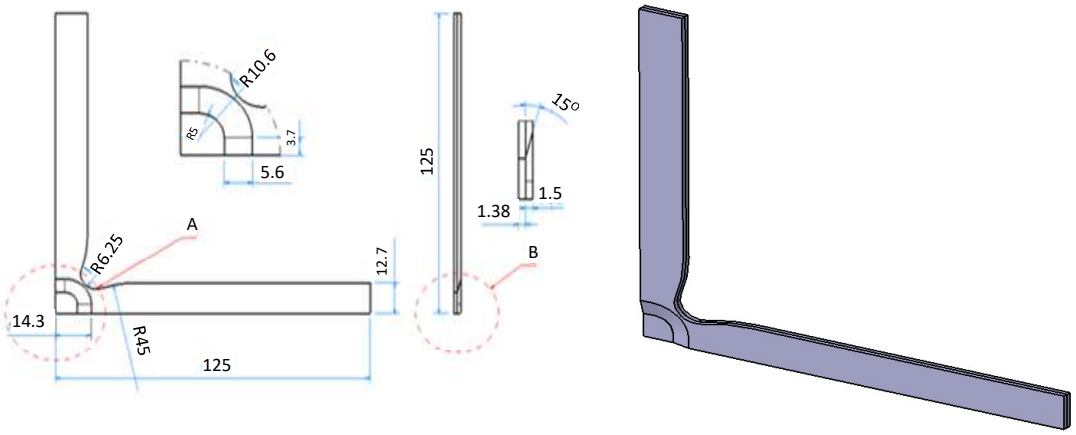

Figure 15. Type D-M1 coupon (dimensions in mm).

The first geometrical modification developed is shown in Fig. 15 (Type D-M1 coupon) and consists of limiting the reduced thickness area just to the central zone of the coupon. To this end, the original tabs were extended to cover the whole coupon, but not the central zone where the failure needs to be located. This modification is expected to reduce the stress concentration at the free edge. The new tabs can be made either of glass (like the previous models), or alternatively, considering the coupon as an entire body made of unidirectional carbon-epoxy laminate. This second option will be more advantageous from the manufacturing point of view.

Fig. 16 shows the σ_{xx} distribution for the 100% carbon D-Type M1 coupon (Type D-M1 (Carbon/Carbon)) and associated with the $n = 1$ case. The results presented show

that the free edge stress concentration is still present although its value (108 MPa) is substantially lower than the one associated with the original Type D coupon (205 MPa).

Moreover, the stress state at the central zone is more uniform than in the previous coupons and σ_{xx} at the centre of the coupon reaches, in this case, 68% of the maximum value ($\sigma_{xx}^{max} / \sigma_{xx}^{centre} = 1.46$, see Table 3). σ_{xx}^{max} is located at both the free edge and the joint between the central zone and the adjacent sloping zone (a transition zone between the central and outer zones) and is probably associated with the local geometry of the coupon. In the case of the glass tabs (Type D-M1 (Carbon/Glass) coupon) the situation is more unfavourable, showing a $\sigma_{xx}^{max} / \sigma_{xx}^{centre}$ ratio of 2.42 (Table 3). As a consequence, only the geometrical modification implemented in the 100% carbon Type D-M1 coupon moves the study closer to its final objective but even this still seems insufficient.

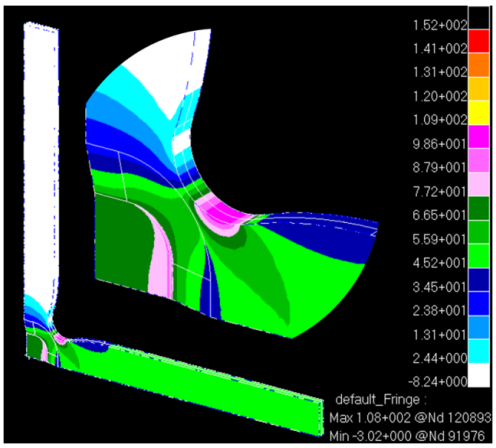

Figure 16. σ_{xx} distribution (MPa) ($n = 1$). (Type D-M1 coupon (Carbon/Carbon)).

Coupon	σ_{xx}^{max}	σ_{xx}^{centre}	$\sigma_{xx}^{max} / \sigma_{xx}^{centre}$
Type D-M1 (Carbon/Carbon)	108	74.098	1.46
Type D-M1 (Carbon/Glass)	152	62.704	2.42
Type D-M2 (Carbon/Carbon)	110*	91.554	1.20
Type D-M3 (Carbon/Carbon)	108*	93	1.16

Table 3. $\sigma_{xx}^{max} / \sigma_{xx}^{centre}$ for Type D-M1, D-M2 and D-M3 coupons ($n = 1$).(*=value measured at the free edge).

The next modification proposed, Type D-M2, is presented in Fig. 17. It consists of the increasing of the 100% carbon Type D-M1 coupon thickness outside of the central zone. The dimensions change from 5.75 mm (Type D-M1) to 7.75 mm (Type D-M2). As a consequence, a 5º increase in the slope of the transition zone is experienced.

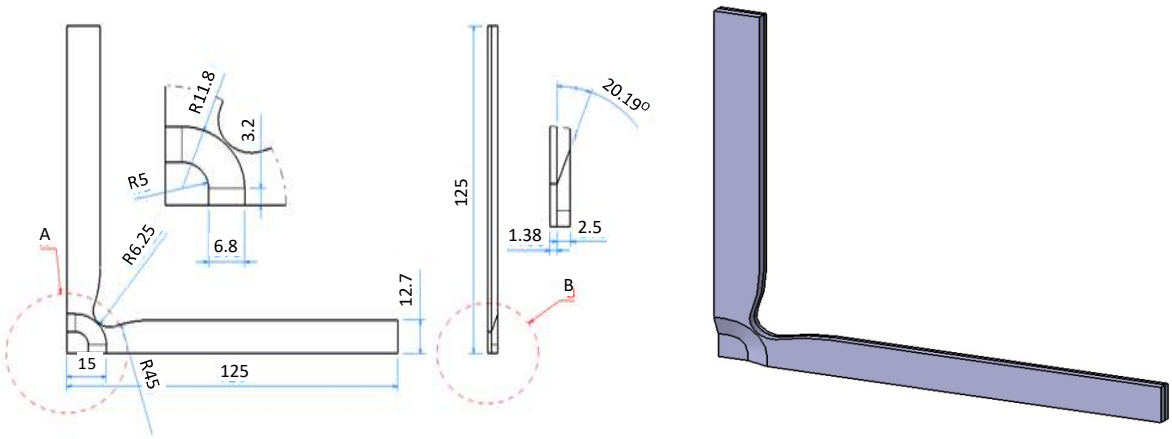

Figure 17. Type D-M2 coupon (dimensions in mm).

Fig. 18 shows the σ_{xx} distribution for the Type D-M2 coupon associated with the $n = 1$ case. The results presented in the Figure show that the free edge stress concentration has approximately the same value as the Type D-M1 coupon (110 MPa), but with a concentration factor of 1.20 (substantially lower than in the Type D-M1 coupon, Table 3). The maximum σ_{xx} value (130MPa) is located now at the joint between the central and the transition zones and is associated with the increase of the slope of the transition zone. In practice, this new concentration will be reduced by the fillet radius that will be unavoidably performed in this intersection by the machining of the central zone during the manufacturing process; in any case, this new concentration

ensures that the initiation of failure will be at the biaxial zone. Another noteworthy result is the quite uniform character of the σ_{xx} distribution in the central zone.

A new modification, Type D-M3, is presented in Fig. 19. Based on Type D-M2, the transition between the central and outer zones is performed by means of a spline leading to a non constant slope area, in an attempt to reduce the concentration at the edge of the transition zone (independently of the fillet radius machined in the real coupon). The slope of the transition zone is reduced now to 13.9º in its outer parts (horizontal and vertical) and to 18º in its central part.

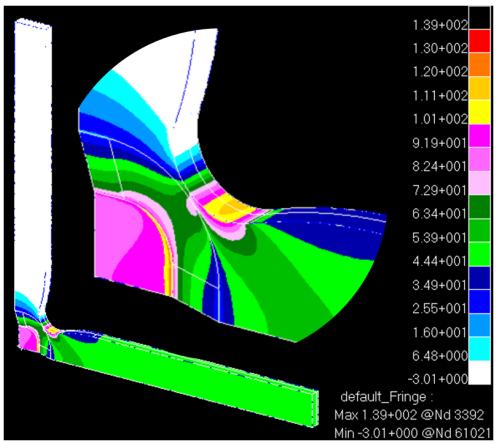

Figure 18. σ_{xx} distribution (MPa) ($n = 1$). (Type D-M2 coupon).

Fig. 20 shows the σ_{xx} distribution for $n = 1$ acting on Type D-M3 coupon. The σ_{xx} values are quite similar to the Type D-M2 values, although slightly lower. The central zone of the coupon is quite uniformly stressed, with values of about 86% of the maximum. The maximum (126 MPa) is detected at the joint between the central and the transition zones, instead of at the outer side of the coupon, as occurred in the Type D-M2 case. The central zone is thus identified as the preferential area for failure occurrence. The concentration factor at the free edge is now 1.16 (Table 3).

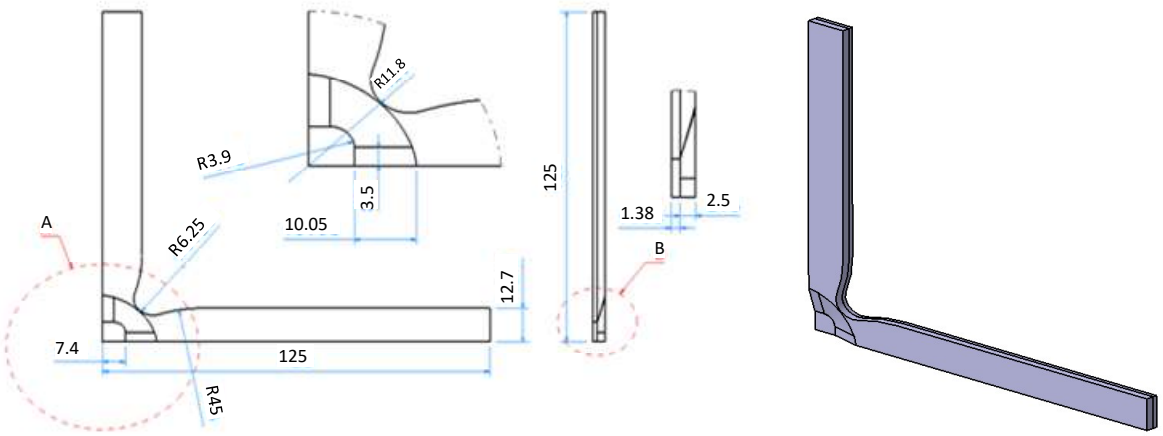

Figure 19. Type D-M3 coupon (dimensions in mm).

Therefore, the results provided by Type D-M3 model are quite satisfactory and improve those shown by Type D-M2 (although not significantly), which points Type D-M3 coupon as an appropriate proposal for the carrying out of transverse tensile biaxial tests. Notice, anyhow, that Type D-M2 coupon seems to require an easier and then more affordable manufacturing process.

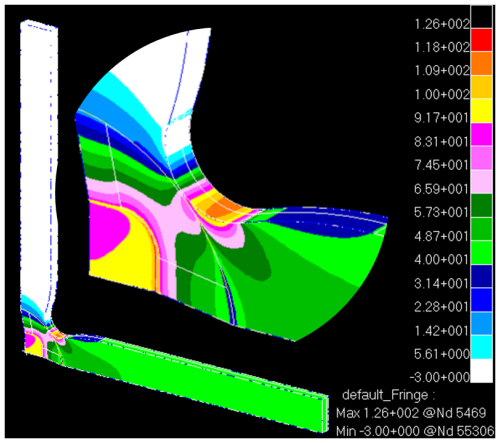

Figure 20. σ_{xx} distribution (MPa) ($n=1$). (Type D-M3 coupon).

5. CONCLUSIONS

FEM models were developed in order to design the coupon best suited for the development of tension-tension biaxial transverse tests.

Four initial models were considered (Types A, B, C and D). The mechanical analysis showed that the main inconvenience of these designs is the remarkable stress concentration that arises in all cases at the free edge. Experimental tests performed at this point confirmed the representativity of the numerical studies.

Based on the former results subsequent geometrical modifications were performed on Type D coupon. These alterations mainly consisted of increasing the thickness associated with the outer part of the central zone; besides, the shape of this central zone was further modified including a variable transition zone slope (Type D-M3 coupon). Stress concentration is noticeably reduced in this last model (Type D-M3). In addition, this coupon presents a quite uniform central stress area. Finally, the maximum σ_{xx} values occur at the joint between the transition zone and the central area; based on this, failure occurrence would be presumably promoted at the biaxial central zone. Based on the results of this paper a testing campaign on the Type D-M geometries is currently in process.

ACKNOWLEDGEMENTS

This study was supported by the Spanish Ministry of Education and Science/Economy and Competitiveness and the Junta de Andalucía (Projects MAT2013-45069-P, MAT2016-80879-P, DPI 2012-37187 and P11-TEP-7093).

REFERENCES

[1] París F, Correa E, Mantič V. Kinking of transverse interface cracks between fibre and matrix. J App Mech 2007; 74(4): 703-716.

[2] Correa E, Gamstedt EK, París F, Mantič V. Effects of the presence of compression in transverse cyclic loading on fibre–matrix debonding in unidirectional composite plies. Compos. Part A 2007; 38: 2260–2269.

[3] Correa E, Mantič V, París F. Effect of thermal residual stresses on matrix failure under transverse tension at micromechanical level: A numerical and experimental analysis. Compos. Sci. Technol. 2011; 71(5): 622-629.

[4] Hashin Z, Rotem A. A fatigue failure criterion for fibre reinforced materials. J. Comp. Mat. 1973;7: 448-464.

[5] París F, Correa E, Cañas J. Micromechanical view of failure of the matrix in fibrous composite materials. Compos Sci Technol 2003; 63: 1041-1052.

[6] Correa E, París F, Mantič V. Effect of the presence of a secondary transverse load on the inter-fibre failure under tension. Eng Fract Mech 2013*;* 103: 174–189.

[7] Barroso A, Correa E, Pérez MD, Vega D, París F. Design of transverse biaxial tensile tests on cruciform specimens. In Proceedings of 19th International Conference on Composite Materials (ICCM19), Montreal, 2013.

[8] Barroso A, Correa E, Freire J, París F. A device for biaxial testing in uniaxial machines. Design, manufacturing and experimental results using cruciform specimens of composite materials, *submitted for publication.*

[9] Welsh JS, Adams DF. An experimental investigation of the biaxial strength of IM6/3501-6 carbon/epoxy cross-ply laminates using cruciform coupons. Compos. Part A 2002; 33: 829-839.

[10] Bhatnagar N, Bhardwaj R, Selvakumar P, Brieu M. Development of a biaxial tensile test fixture for reinforced thermoplastic composites. Polym. Test. 2007; 26: 154-161.

[11] Smits A, Van Hemelrijck D, Philippidis TD, Cardon A. Design of a cruciform coupon for biaxial testing of fibre reinforced composite laminates. Compos. Sci. Technol. 2006;66: 964–975.

[12] Lamkanfi E, Van Paepegem W, Degrieck J, Ramault C, Makris A, Van Hemelrijck

D. Strain distribution in cruciform coupons subjected to biaxial loading conditions. Part 1: two-dimensional versus three-dimensional finite element model. Polym. Test. 2010; 29(1): 7-13.

[13] Lamkanfi E, Van Paepegem W, Degrieck J, Ramault C, Makris A, Van Hemelrijck D. Strain distribution in cruciform coupons subjected to biaxial loading conditions. Part 2: Influence of geometrical discontinuities. Polym. Test. 2010; 29(1): 132-138.

[14] Makris A, Vandenbergh T, Ramault C, Van Hemelrijck D, Lamkanfi E. and Van Paepegem, W. Shape optimisation of a biaxially loaded cruciform specimen, Polym. Test. 2010; 29(1): 216-223.

[15] Escárpita, A., Elizalde, H., Ramı´rez, R.A., Ledezma, E. and Pinho, S.T. (2009). Modified Cruciform Specimen for Biaxial Testing of Fibre-reinforced Composites, in: Proceedings of the 17th International Conference on Composite Materials (ICCM-17), Edinburgh, 2009.

[16] Huang H, Sung KH, KOYANAGI J, Melo JD, Kumazawa H. and Susuki I. Effects of an Open Hole on the Biaxial Strengths of Composite Laminates. J. Comp. Mat. 2010; 44:2429-2445

[17] Soden PD, Hinton MJ and Kaddour AS. Lamina properties, lay-up configurations and loading conditions for a range of fibre-reinforced composite laminates, Compos. Sci. Technol. 1998;58:1011-1022.

[18] Puck A, Schürmann H. Failure analysis of FRP laminates by means of physically based phenomenological model. Compos Sci Technol 1998;58:1045–67.